On the basis of our results, combined with previous studies, we propose a model for the ion flux pathway through MotA/B and PomA/B ion channels (Fig. 8). First, the ion passes through the periplasmic side of a channel pore, a part of which is formed by Leu183 of PomA and Cys31 of PomB, or Met206 of MotA and Ala39 of MotB (Sudo *et al.*, 2009b). Next, the ion binds to the pocket that is formed mainly by Asn194 of PomA and Asp24 of PomB, or by Tyr217 of MotA and Asp32 of MotB (Sudo *et al.*, 2009b; Terashima *et al.*, 2010). Finally, an event to generate torque starts, and the ion is released from the ion binding pocket to the cytoplasm, and at this stage, Phe22 of PomB or Tyr30 of MotB might be important. In this study, we introduced mutations into TM4 of PomA or into the TM of PomB. To convert from the Na^+ to the H^+ type, mutations need to be introduced in residues of PomA TM1, 2 or 3, and the mutations need to be combined.

ACKNOWLEDGEMENTS

This work was supported in part by grants-in-aid for scientific research from the Ministry of Education, Science, and Culture of Japan, the Japan Science and Technology Corporation (to M. H. and to S. K.), the Soft Nano-Machine Project of the Japan Science and Technology Agency (to M. H.) and the Japan Society for the Promotion of Science (to H. T.).

REFERENCES

Asai, Y., Kojima, S., Kato, H., Nishioka, N., Kawagishi, I. & Homma, M. (1997). Putative channel components for the fast-rotating sodium-driven flagellar motor of a marine bacterium. *J Bacteriol* **179**, 5104–5110.

Asai, Y., Kawagishi, I., Sockett, R. E. & Homma, M. (2000). Coupling ion specificity of chimeras between H^+- and Na^+-driven motor proteins, MotB and PomB, in *Vibrio* polar flagella. *EMBO J* **19**, 3639–3648.

Asai, Y., Yakushi, T., Kawagishi, I. & Homma, M. (2003). Ion-coupling determinants of Na^+-driven and H^+-driven flagellar motors. *J Mol Biol* **327**, 453–463.

Blair, D. F. & Berg, H. C. (1990). The MotA protein of *E. coli* is a proton-conducting component of the flagellar motor. *Cell* **60**, 439–449.

Braun, T. F. & Blair, D. F. (2001). Targeted disulfide cross-linking of the MotB protein of *Escherichia coli*: evidence for two H^+ channels in the stator complex. *Biochemistry* **40**, 13051–13059.

Braun, T. F., Al-Mawsawi, L. Q., Kojima, S. & Blair, D. F. (2004). Arrangement of core membrane segments in the MotA/MotB proton-channel complex of *Escherichia coli*. *Biochemistry* **43**, 35–45.

Chun, S. Y. & Parkinson, J. S. (1988). Bacterial motility: membrane topology of the *Escherichia coli* MotB protein. *Science* **239**, 276–278.

Dean, G. E., Macnab, R. M., Stader, J., Matsumura, P. & Burks, C. (1984). Gene sequence and predicted amino acid sequence of the *motA* protein, a membrane-associated protein required for flagellar rotation in *Escherichia coli*. *J Bacteriol* **159**, 991–999.

Fukuoka, H., Yakushi, T., Kusumoto, A. & Homma, M. (2005). Assembly of motor proteins, PomA and PomB, in the Na^+-driven stator of the flagellar motor. *J Mol Biol* **351**, 707–717.

Gouaux, E. & Mackinnon, R. (2005). Principles of selective ion transport in channels and pumps. *Science* **310**, 1461–1465.

Guzman, L. M., Belin, D., Carson, M. J. & Beckwith, J. (1995). Tight regulation, modulation, and high-level expression by vectors containing the arabinose PBAD promoter. *J Bacteriol* **177**, 4121–4130.

Hunte, C., Screpanti, E., Venturi, M., Rimon, A., Padan, E. & Michel, H. (2005). Structure of a Na^+/H^+ antiporter and insights into mechanism of action and regulation by pH. *Nature* **435**, 1197–1202.

Ito, M., Terahara, N., Fujinami, S. & Krulwich, T. A. (2005). Properties of motility in *Bacillus subtilis* powered by the H^+-coupled MotAB flagellar stator, Na^+-coupled MotPS or hybrid stators MotAS or MotPB. *J Mol Biol* **352**, 396–408.

Jaques, S., Kim, Y. K. & McCarter, L. L. (1999). Mutations conferring resistance to phenamil and amiloride, inhibitors of sodium-driven motility of *Vibrio parahaemolyticus*. *Proc Natl Acad Sci U S A* **96**, 5740–5745.

Kawagishi, I., Okunishi, I., Homma, M. & Imae, Y. (1994). Removal of the periplasmic DNase before electroporation enhances efficiency of transformation in the marine bacterium *Vibrio alginolyticus*. *Microbiology* **140**, 2355–2361.

Kojima, S. & Blair, D. F. (2001). Conformational change in the stator of the bacterial flagellar motor. *Biochemistry* **40**, 13041–13050.

Kojima, S. & Blair, D. F. (2004). Solubilization and purification of the MotA/MotB complex of *Escherichia coli*. *Biochemistry* **43**, 26–34.

Kojima, S., Asai, Y., Atsumi, T., Kawagishi, I. & Homma, M. (1999). Na^+-driven flagellar motor resistant to phenamil, an amiloride analog, caused by mutations in putative channel components. *J Mol Biol* **285**, 1537–1547.

Kojima, S., Shoji, T., Asai, Y., Kawagishi, I. & Homma, M. (2000). A slow-motility phenotype caused by substitutions at residue Asp31 in the PomA channel component of a sodium-driven flagellar motor. *J Bacteriol* **182**, 3314–3318.

Kojima, S., Imada, K., Sakuma, M., Sudo, Y., Kojima, C., Minamino, T., Homma, M. & Namba, K. (2009). Stator assembly and activation mechanism of the flagellar motor by the periplasmic region of MotB. *Mol Microbiol* **73**, 710–718.

Leake, M. C., Chandler, J. H., Wadhams, G. H., Bai, F., Berry, R. M. & Armitage, J. P. (2006). Stoichiometry and turnover in single, functioning membrane protein complexes. *Nature* **443**, 355–358.

Lloyd, S. A. & Blair, D. F. (1997). Charged residues of the rotor protein FliG essential for torque generation in the flagellar motor of *Escherichia coli*. *J Mol Biol* **266**, 733–744.

Murata, T., Yamato, I., Kakinuma, Y., Leslie, A. G. & Walker, J. E. (2005). Structure of the rotor of the V-type Na^+-ATPase from *Enterococcus hirae*. *Science* **308**, 654–659.

Murata, T., Yamato, I., Kakinuma, Y., Shirouzu, M., Walker, J. E., Yokoyama, S. & Iwata, S. (2008). Ion binding and selectivity of the rotor ring of the Na^+-transporting V-ATPase. *Proc Natl Acad Sci U S A* **105**, 8607–8612.

Okabe, M., Yakushi, T., Asai, Y. & Homma, M. (2001). Cloning and characterization of *motX*, a *Vibrio alginolyticus* sodium-driven flagellar motor gene. *J Biochem* **130**, 879–884.

Okunishi, I., Kawagishi, I. & Homma, M. (1996). Cloning and characterization of *motY*, a gene coding for a component of the sodium-driven flagellar motor in *Vibrio alginolyticus*. *J Bacteriol* **178**, 2409–2415.

Reid, S. W., Leake, M. C., Chandler, J. H., Lo, C. J., Armitage, J. P. & Berry, R. M. (2006). The maximum number of torque-generating units in the flagellar motor of *Escherichia coli* is at least 11. *Proc Natl Acad Sci U S A* **103**, 8066–8071.

Sato, K. & Homma, M. (2000a). Functional reconstitution of the Na^+-driven polar flagellar motor component of *Vibrio alginolyticus*. *J Biol Chem* **275**, 5718–5722.

Sato, K. & Homma, M. (2000b). Multimeric structure of PomA, a component of the Na^+-driven polar flagellar motor of *Vibrio alginolyticus*. *J Biol Chem* **275**, 20223–20228.

Stader, J., Matsumura, P., Vacante, D., Dean, G. E. & Macnab, R. M. (1986). Nucleotide sequence of the *Escherichia coli motB* gene and site-limited incorporation of its product into the cytoplasmic membrane. *J Bacteriol* **166**, 244–252.

Sudo, Y., Kitade, Y., Furutani, Y., Kojima, M., Kojima, S., Homma, M. & Kandori, H. (2009a). Interaction between Na^+ ion and carboxylates of the PomA-PomB stator unit studied by ATR-FTIR spectroscopy. *Biochemistry* **48**, 11699–11705.

Sudo, Y., Terashima, H., Abe-Yoshizumi, R., Kojima, S. & Homma, M. (2009b). Comparative study of the ion flux pathway in stator units of proton- and sodium-driven flagellar motors. *Biophysics (J-STAGE)* **5**, 45–52.

Tao, X., Lee, A., Limapichat, W., Dougherty, D. A. & MacKinnon, R. (2010). A gating charge transfer center in voltage sensors. *Science* **328**, 67–73.

Terahara, N., Krulwich, T. A. & Ito, M. (2008). Mutations alter the sodium versus proton use of a *Bacillus clausii* flagellar motor and confer dual ion use on *Bacillus subtilis* motors. *Proc Natl Acad Sci U S A* **105**, 14359–14364.

Terashima, H., Kojima, S. & Homma, M. (2008). Flagellar motility in bacteria structure and function of flagellar motor. *Int Rev Cell Mol Biol* **270**, 39–85.

Terashima, H., Kojima, S. & Homma, M. (2010). Functional transfer of an essential aspartate for the ion-binding site in the stator proteins of the bacterial flagellar motor. *J Mol Biol* **397**, 689–696.

Yakushi, T., Maki, S. & Homma, M. (2004). Interaction of PomB with the third transmembrane segment of PomA in the Na^+-driven polar flagellum of *Vibrio alginolyticus*. *J Bacteriol* **186**, 5281–5291.

Yamashita, A., Singh, S. K., Kawate, T., Jin, Y. & Gouaux, E. (2005). Crystal structure of a bacterial homologue of Na^+/Cl^--dependent neurotransmitter transporters. *Nature* **437**, 215–223.

Yanisch-Perron, C., Vieira, J. & Messing, J. (1985). Improved M13 phage cloning vectors and host strains: nucleotide sequences of the M13mp18 and pUC19 vectors. *Gene* **33**, 103–119.

Yorimitsu, T., Sato, K., Asai, Y., Kawagishi, I. & Homma, M. (1999). Functional interaction between PomA and PomB, the Na^+-driven flagellar motor components of *Vibrio alginolyticus*. *J Bacteriol* **181**, 5103–5106.

Yorimitsu, T., Sowa, Y., Ishijima, A., Yakushi, T. & Homma, M. (2002). The systematic substitutions around the conserved charged residues of the cytoplasmic loop of Na^+-driven flagellar motor component PomA. *J Mol Biol* **320**, 403–413.

Yorimitsu, T., Kojima, M., Yakushi, T. & Homma, M. (2004). Multimeric structure of the PomA/PomB channel complex in the Na^+-driven flagellar motor of *Vibrio alginolyticus*. *J Biochem* **135**, 43–51.

Zhang, X. Y., Goemaere, E. L., Thomé, R., Gavioli, M., Cascales, E. & Lloubès, R. (2009). Mapping the interactions between *Escherichia coli* Tol subunits: rotation of the TolR transmembrane helix. *J Biol Chem* **284**, 4275–4282.

Zhou, J. & Blair, D. F. (1997). Residues of the cytoplasmic domain of MotA essential for torque generation in the bacterial flagellar motor. *J Mol Biol* **273**, 428–439.

Zhou, J., Fazzio, R. T. & Blair, D. F. (1995). Membrane topology of the MotA protein of *Escherichia coli*. *J Mol Biol* **251**, 237–242.

Zhou, J., Lloyd, S. A. & Blair, D. F. (1998a). Electrostatic interactions between rotor and stator in the bacterial flagellar motor. *Proc Natl Acad Sci U S A* **95**, 6436–6441.

Zhou, J., Sharp, L. L., Tang, H. L., Lloyd, S. A., Billings, S., Braun, T. F. & Blair, D. F. (1998b). Function of protonatable residues in the flagellar motor of *Escherichia coli*: a critical role for Asp 32 of MotB. *J Bacteriol* **180**, 2729–2735.

Edited by: P. W. O'Toole

Lasers Med Sci (2013) 28:891–900
DOI 10.1007/s10103-012-1164-6

ORIGINAL ARTICLE

Automatic laser scanning ablation system for high-precision treatment of brain tumors

Hongen Liao · Keisuke Fujiwara · Takehiro Ando · Takashi Maruyama · Etsuko Kobayashi · Yoshihiro Muragaki · Hiroshi Iseki · Ichiro Sakuma

Received: 5 May 2012 / Accepted: 12 July 2012 / Published online: 4 August 2012

Abstract Complete removal of malignant gliomas is important for the prognosis in neurosurgery treatment. Currently, the challenge is how to detect any remaining tumors and resect them during the operation. We have developed a laser ablation system with accurate tumor analysis and fluorescence guidance for high-precision brain tumor resection during neurosurgery. A 5-aminolevulinic acid-induced fluorescent protoporphyrins IX (PpIX)-based intra-operative fluorescence measurement and corresponding spectra analysis technique is used to identify the position of tumors. A galvano mirror scanning mechanism is integrated into the fluorescence measurement and the laser ablation devices for automatic tumor area scanning and corresponding laser ablation. A set of phantom experiments was performed to evaluate the proposed system. Results showed that the galvano scanning mechanism enabled both PpIX fluorescence detection and laser ablation in the same optical axis. In vitro experiments using porcine brain were performed to evaluate the effectiveness of the automatic laser scanning, fluorescence detection, and laser ablation system. The proposed fluorescence-guided laser ablation system can provide accurate analysis and high-precision treatment for tumor resection in neurosurgery. With further improvement, the system can be used in neurosurgical implementation to provide accurate, safe, and simple surgical diagnosis and therapy.

Keywords Laser ablation · Neurosurgery · 5-aminolevulinic-acid · Fluorescence · Spectra analysis

H. Liao (✉) · K. Fujiwara · T. Ando · E. Kobayashi · I. Sakuma
Graduate School of Engineering, The University of Tokyo,
7-3-1 Hongo, Bunkyo-ku,
Tokyo 113-8656, Japan
e-mail: liao@bmpe.t.u-tokyo.ac.jp

H. Liao · E. Kobayashi · I. Sakuma
Translational Systems Biology and Medicine Initiative,
The University of Tokyo,
7-3-1 Hongo, Bunkyo-ku,
Tokyo 113-8656, Japan

H. Liao
School of Medicine, Tsinghua University,
Beijing 10084, China

T. Maruyama · Y. Muragaki · H. Iseki
Graduate School of Medicine,
Tokyo Women's Medical University,
8-1 Kawada-cho, Shinjuku-ku,
Tokyo 162-8666, Japan

Introduction

Malignant gliomas are the most common type of primary brain tumor. While primary malignant brain tumors account for just 2 % of all adult cancers, these tumors cause a huge burden in long-term of disability and death [1]. The symptoms, prognosis, and treatment for malignant gliomas depend on the cell type, grade of malignancy, and location of tumor within the brain. Determining how to completely remove malignant gliomas during neurosurgery is crucial because it affects the overall prognosis of the treatment. Surgeons can resect

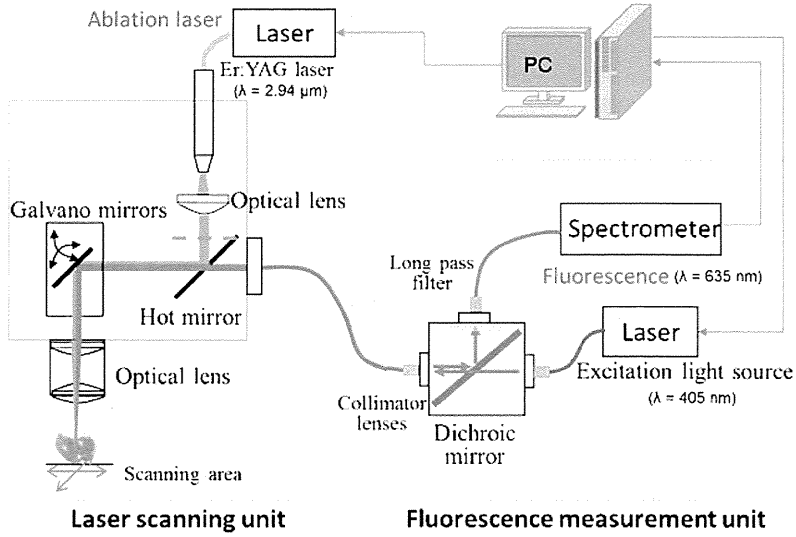

Fig. 1 System configuration

most tumors with an accuracy of millimeters by using a combination of conventional surgical instruments and diagnostic images [2, 3]. Although magnetic resonance (MR) and computed tomography (CT) images can provide surgeons with pre-/intra-operative diagnosis information, some tumor cells remain in the areas adjacent to the tumor removal area and can negatively affect both the diagnosis outcome and the precision of the treatment. It is not enough for surgeons to distinguish the edges of the tumor only using conventional surgical techniques because of the uncertainty involved in identifying viable tumor margins during surgery. In order to perform a complete tumor resection, the accuracy of intra-operative tumor detection and diagnosis needs to be improved.

In a previous study, a 5-aminolevulinic acid (5-ALA)-induced protoporphyrins IX (PpIX) fluorescence was used for intra-operative visualization of malignant glioma tissue [4]. Using the 5-ALA leads to intracellular accumulation of fluorescent PpIX in malignant gliomas and enables intra-operative visualization of malignant gliomas tissue. Other studies have shown that fluorescence can be used to identify residual malignant glioma intra-operatively, thus improving the accuracy of surgical treatment [5–8]. With the guidance of 5-ALA-induced fluorescence in neurosurgery, surgeons can resect a tumor more accurately and intuitively [9, 10].

To achieve a complete resection of tumor tissue, tumor ablation accuracy during treatment is required. The use of laser ablation enables a smooth, precise treatment for small and/or remaining tumors [11]. Laser photocoagulation provides a noncontact therapeutic method with a sub-millimeter accuracy [12, 13]; moreover, the power and the photocoagulation time of the laser is easy to control, thus enabling a more complete tumor removal.

An integrated diagnosis and therapeutic system has been developed for high-precision malignant glioma resection using a 5-ALA-induced fluorescence PpIX-based intra-operative tumor diagnosis technique combined with a laser ablation technique that features an autofocus (AF) mechanism [14, 15]. The boundary between tumorous and nontumorous tissue is identified using 5-ALA-induced PpIX fluorescence and the tumor is then accurately ablated with the micro laser. Combining the 5-ALA fluorescence guidance with high-precision spectral analysis results in higher tumor identification accuracy than with a system that uses only pre-/intra-operative MR imaging [16]. However, the fluorescence

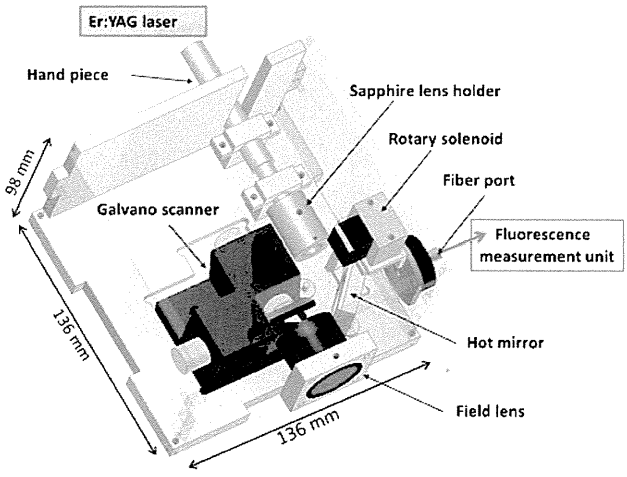

Fig. 2 Design of laser scanning unit

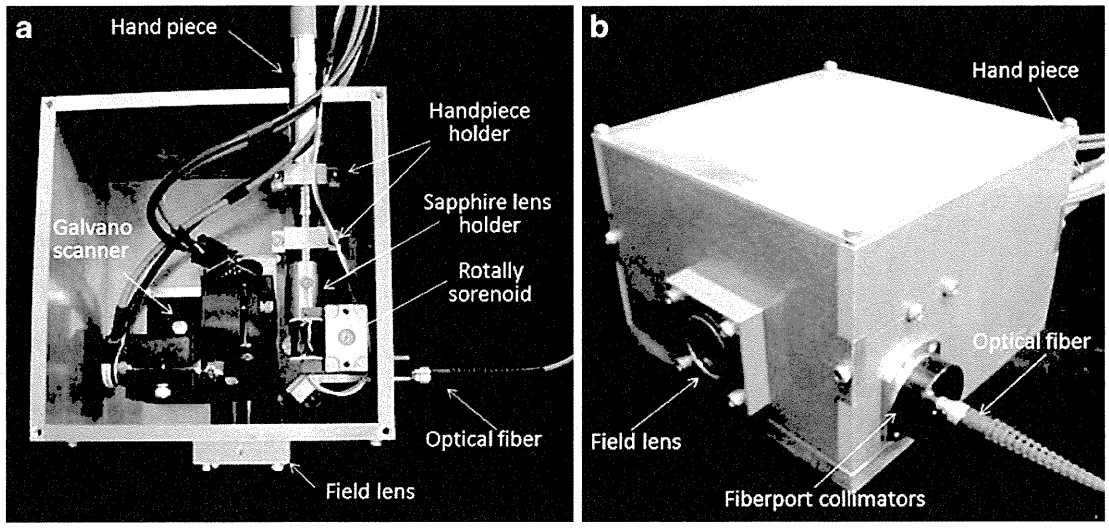

Fig. 3 Manufactured laser scanning unit. **a** Galvano scanning mechanism and laser ablation guidance device; **b** compacted laser scanning unit that can be mounted to a robotic arm during neurosurgery

measurement device and the laser ablation device were separated. The entire tumor was first scanned and the tumor area was indentified. Laser ablation was performed after fluorescence spectral analysis. Although experiments have demonstrated that it is possible to use an AF device mounted on a robotic manipulator, the spectral analysis and laser ablation could not be performed simultaneously. Because deformation and movement of the brain tissue occurs during the surgical procedure, the nonsimultaneous preformation of diagnosis and therapy affects the accuracy of tumor resection.

To address these issues, we developed a new mechanism with the same optical path for the excitation laser used in fluorescence measurement and the ablation laser used for tumor laser photocoagulation. Our coaxial system includes an automatic laser scanning mechanism for automatic fluorescence measurement and laser ablation when the direction of the lasers is needed to be changed. The rest of this paper is organized as follows. In the "Methods and system configuration" section, we describe the requirements of fluorescence-guided laser ablation for neurosurgery, the system configuration, and the details of each unit. In the "Experiments and results" section, we present our automatic laser scanning ablation device and a set of experiments we performed to assess the laser photocoagulation as well as our analysis of the fluorescence spectra. An in vitro experiment using porcine brain tissue is also described in this section. We discuss possible extensions to the method and conclude with a brief summary in "Discussion and conclusion" section.

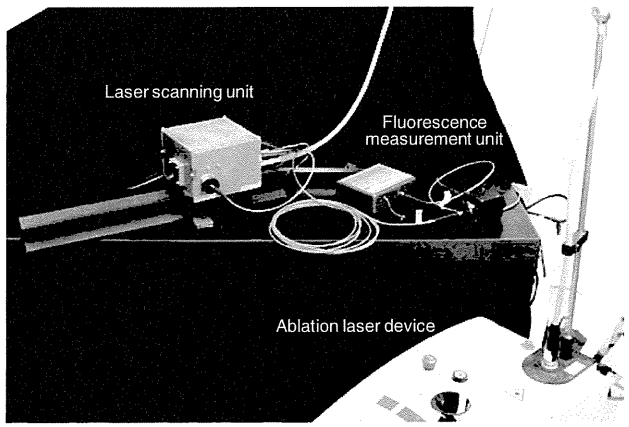

Fig. 4 Prototype of the fluorescence measurement and laser ablation device

Methods and system configuration

We develop a coaxial fluorescence measurement with and laser ablation system for accurate analysis of tumor and high-precision brain tumor resection during neurosurgery. In this section, we describe the system requirements related to fluorescence-guided laser ablation for neurosurgery, the system configuration, the fluorescence measurement and analysis, the laser scanning mechanism, and the laser ablation device.

Requirements of fluorescence-guided laser ablation for neurosurgery

Although combining diagnosis imaging techniques (such as MRI and CT) can improve tumor acquisition,

Table 1 Laser power transmission efficiency (n=10)

Positions of Er: YAG laser	20 Hz–50 mJ	20 Hz–75 mJ	20 Hz–100 mJ	10 Hz–100 mJ
Tip of hand piece	99.6±0.5	97.2±0.4	98.2±0.3	98.2±0.4
Sapphire lens	85.8±0.5	85.3±0.4	85.8±0.5	86.4±0.6
Objective lens	66.9±0.5	65.4±0.3	66.6±0.4	67.2±0.6

performance, accurate, real-time tumor identification is still required. Using 5-ALA-induced PpIX fluorescence enables high-precision identification of the tumor surface, which is then used to precisely identify small tumors or residual tumor tissue during an operation, thereby providing guidance for laser ablation. With the integration of a laser ablation device, the system can be used for precision intra-operative treatment for blurry boundaries between healthy brain tissue and brain tumor that may contain a tumor. There are four main requirements for using fluorescence-guided laser ablation in neurosurgery: (1) the working distance from the scanning plane should be about 20 mm, (2) the laser scanning unit should be mounted on a neurosurgery robotic arm in the operation room, (3) the laser scanning range for small tumors should be about 10 mm×10 mm, (4) the diameter of the laser spot ablated on the tumor should be less than 2 mm, and (5) laser photocoagulation should only be performed on a tumor with the guidance of fluorescence.

System configuration

The proposed fluorescence-guided automatic laser ablation system includes a fluorescence measurement unit, a laser scanning unit, and a PC for fluorescence spectra analysis and ablation laser control (Fig. 1). The PC is used to control the fluorescence measurement and laser scanning units. Data received from a spectrometer is also analyzed by the PC. These analyzed results are then used to determine whether or not the scanned area is tumor tissue. The laser scanning unit has two functions: one for fluorescence measurement scanning and the other for laser ablation scanning. The laser scanning and tumor ablation procedure consists of four parts: (1) an excitation light (blue–violet light, λ=405 nm) is used to excite the PpIX so that a brain tumor is easy to spot by the red fluorescence it emits, (2) a spectroscope is used to collect excited fluorescence, which is then analyzed by PC, (3) if the area is identified as containing tumor tissues, a hot mirror is angled downward so that the Er:YAG laser can be trained on the target area, and (4) the fluorescence analysis and laser ablation procedure with the galvano mirror scanning mechanism are repeated so that all the required area can be scanned.

Fluorescence measurement unit

As a metabolic precursor in the heme biosynthesis pathway, 5-ALA elicits and induces the synthesis of PpIX, which tends to accumulate in pathological lesions. When it is excited by blue-violet light (wavelength of about 405 nm), brain tumors are easy to spot due to the PpIX emitting a red fluorescence (wavelength of about 635 nm). In this system, we selected a laser diode with a wavelength of 406 nm (GH04125A2AE, SHARP Co., Maximum output: 150 mW) connected by a fiber as a light source. A spectrometer (WTC-111E; B&W TEK Inc.; wavelength measurement range, 300–850 nm) was used to measure the spectrum. The exposure time of the spectrometer can be controlled by PC. We use a

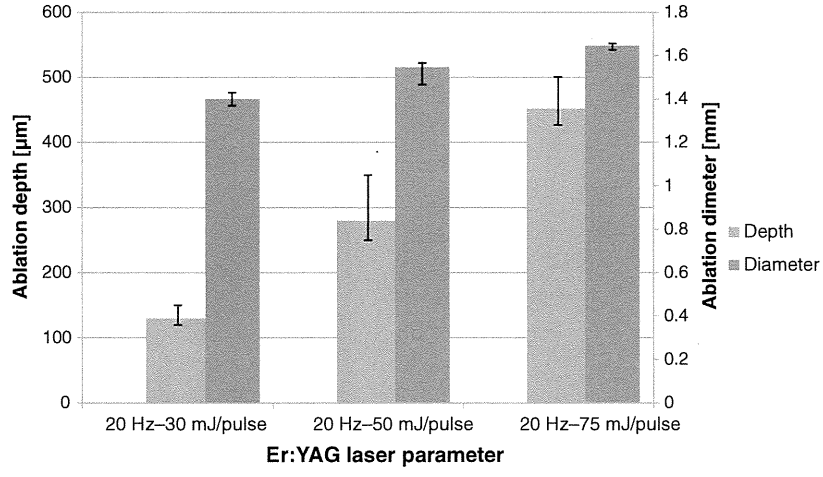

Fig. 5 Laser photocoagulation efficiency with same repetition frequency (20 Hz) and different pulse energies (30, 50, 75 mJ/pulse)

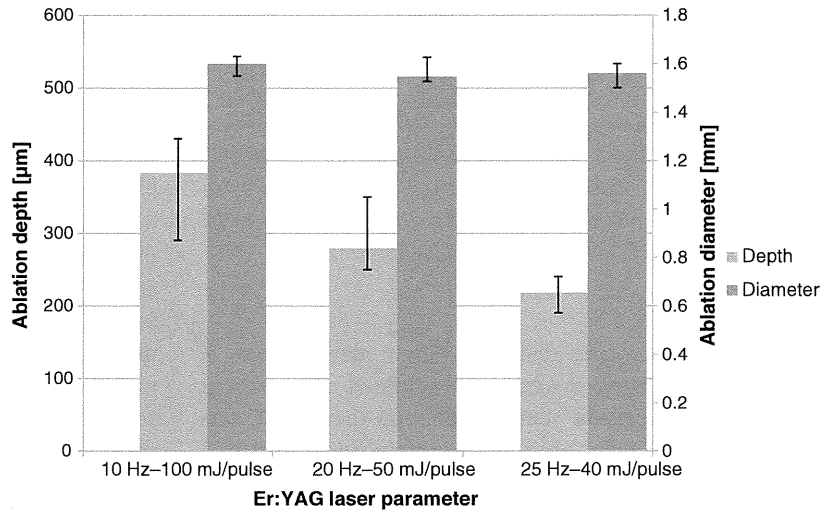

Fig. 6 Laser photocoagulation efficiency with different repetition frequencies and pulse energies. The total laser power output was the same

dichroic mirror (cutoff wavelength, 550 nm) to combine the optical path for optical fiber (core diameter, 365 μm) so that the excitation light and the fluorescence can be guided by a single fiber.

As shown in the fluorescence measurement unit in Fig. 1, the laser scanning unit is connected with the spectrometer and the excitation light source with a fiber. Since the excitation light and the fluorescence are transmitted by the same fiber, the fluorescence is only obtained from the excited area of PpIX. In order to decrease the strong reflected excitation light that cannot be avoided by dichroic mirror, we inserted a long pass filter with a cutoff wavelength of 550 nm between the mirror and the spectrometer.

Laser scanning unit

Figure 2 shows the design of the laser scanning unit. An Er:YAG laser device (ER-M1TH; HOYA Photonics Inc.) was used for tumor laser photocoagulation. This device enables a laser output of oscillator pulse repetition frequency (selectable from 3, 10, 20, 25, or 30 Hz) and pulse energy (30–350 mJ/pulse). A galvano mirror scanner (6220 H, Cambridge Technology Inc.) was integrated into the laser scanning mechanism. The direction of the excitation light and the Er:YAG laser can be changed by the controlling the angle of the galvanometer mirror so that the tumor area can be scanned automatically without changing the position and orientation of the entire device.

A hot mirror (gold mirror) is placed in front of the galvanometer scanner to switch the optical path. During the fluorescence measurement, the mirror is angled upward so that the fluorescence can pass through the fluorescence measurement unit to the galvano scanning device directly. In the laser photocoagulation procedure, the mirror is angled downward so that the ablation laser can be reflected to the galvano scanning

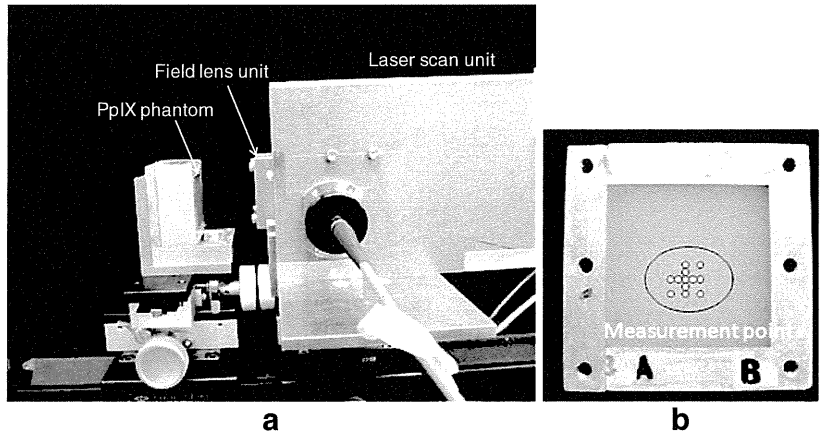

Fig. 7 Fluorescence measurement for different points; **a** experimental device; **b** measurement points

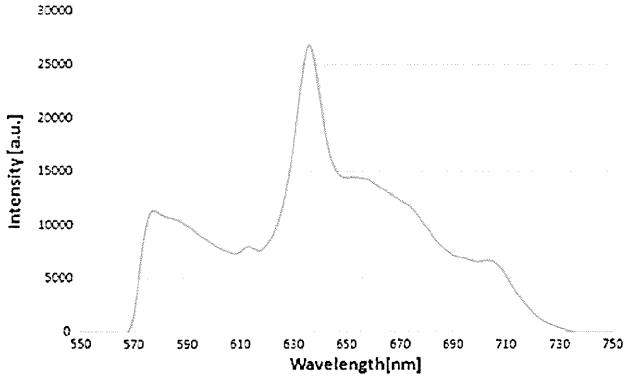

Fig. 8 Results of fluorescence spectrum

device. When the light from the galvano mirror passes through the objective lens and is irradiated to the target surface, although the two lights have the same angle during both the fluorescence measurement and the laser ablation, they have different focus points due to the chromatic dispersion caused by the large difference in wavelength. We should be able to correct the irradiation angle of the Er:YAG laser by enlarging the irradiation slightly. The optimum correction angle can be determined by ray tracking simulation.

The manufactured laser scanning mechanism is shown in Fig. 3a. The device is compact enough to be mounted on a robotic arm during neurosurgery (Fig. 3b).

Experiments and results

We manufactured the laser scanning device and combined it with the fluorescence measurement device (Fig. 4). A set of experiments were then performed to evaluate the system using a biomedical stimulant phantom and a porcine brain. During experimentation, the developed laser scanning unit was fixed to an optical rail.

Evaluation of Er:YAG laser power transmission efficiency

First, we evaluated the stability of the Er:YAG laser emitted from the objective lens of the laser scanning unit. The transmission efficiency of the laser power was also measured at three positions: tip of hand piece, sapphire lens, and output position after passing the objective lens. Four combinations of different repetition frequencies and pulse energies (20 Hz–50 mJ, 20 Hz–75 mJ, 20 Hz–100 mJ, 10 Hz–100 mJ) were carried out to evaluate the laser power output. Each test of 5 s per irradiation was performed for 10 measurements.

The results of the laser power measurements are shown in Table. 1. About 65–67 % laser power was transmitted to the target surface regardless of the parameter setting which indicates that the laser power transmission efficiency was stable. In addition, the theoretical value of the transmission efficiency of the laser power was also about 69 %, which is almost equal to the transmission efficiency we experimentally obtained.

Evaluation of Er:YAG laser photocoagulation efficiency

To evaluate the Er:YAG laser photocoagulation efficiency with different repetition frequencies and pulse energies, we constructed a biomedical phantom that could simulate the optical scattering properties of brain tissue. The Er:YAG was applied to the phantom, and we then measured the size and depth of the hole created by the laser irradiation. Five sets of experiments with different combinations of repetition frequency and pulse energy (20 Hz–30 mJ, 20 Hz–50 mJ, 20 Hz–75 mJ, 10 Hz–100 mJ, 25 Hz–40 mJ) were performed.

Figure 5 shows the results of the Er:YAG laser photocoagulation efficiency evaluation. In the case of repetition frequency of 20 Hz, the depth and diameter of the irradiation spot were increased by the increased pulse

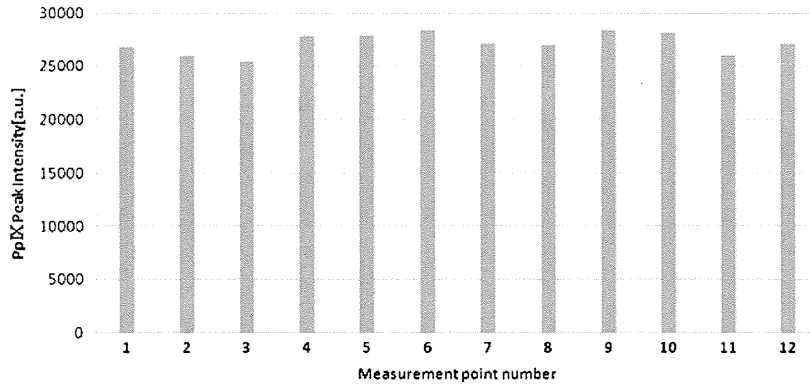

Fig. 9 PpIX peak intensity for 12 measurement points

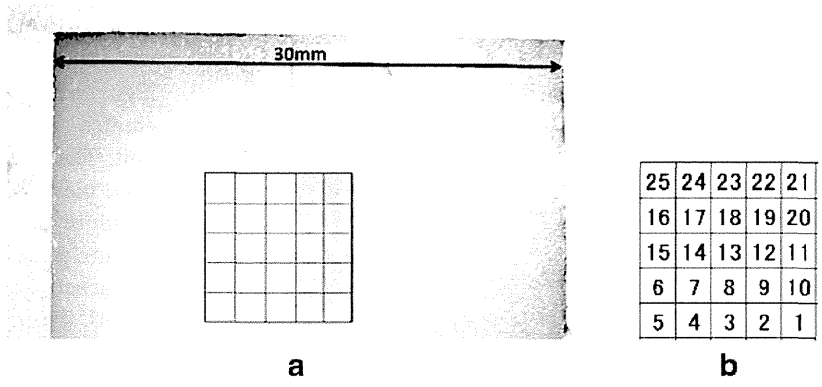

Fig. 10 Results of integrated evaluation experiment with 25 measurement points. **a** Measurement area that received laser ablation from the right-hand side; **b** Corresponding measurement number

energy. We also evaluated a laser power output of 1 W with different combinations (10 Hz–100 mJ, 20 Hz–50 mJ, 25 Hz–40 mJ). The results showed that a smaller repetition frequency enabled a deeper irradiation depth (Fig. 6).

Evaluation of fluorescence spectra analysis

We performed spectral measurements at 12 points in the phantom by changing the angle of the galvano mirrors. The phantom was made of a solution of 1 ml PpIX (concentration, 200 μg/ml). Exposure time of the spectrometer was 500 ms and output of the excitation light was 7.5 mW. The experimental devices and measurement points are shown in Fig. 7.

Figure 8 shows the result of spectral measurements of fluorescence spectrum. The fluorescence peak wavelength was 635 nm. The PpIX peak intensity for all 12 measurement points is shown in Fig. 9. The average peak intensity was 27,200 a.u. with a standard deviation of 980 a.u. These results show that the peak of the PpIX fluorescence could be detected by controlling the angle of the excitation laser using the galvano scanner.

Evaluation of integration of fluorescence measurement and laser ablation

We conducted a set of combined experiments to evaluate the integrated system of fluorescence spectra analysis and corresponding laser ablation. The objective of this experiment was to determine whether the peak area of 5-ALA-induced PpIX could be laser photocoagulated automatically by the Er:YAG laser. We manufactured an agar plate containing Intralipid-10 % as an optical simulant material for brain tissue. The concentration of Intralipid-10 % was set so that the scattering coefficient (us1) was 3 cm^{-1} in the PpIX area and 30 cm^{-1} in the other area, which are values similar to those of glioma and white matter.

The spot diameters of the excitation laser and the Er:YAG laser were about 1.6 mm. We constructed two phantoms with a laser scanning area of 8 mm×8 mm covering 25 points and 10 mm×10 mm covering 36 points for the fluorescence measurements and the laser ablations, respectively. The output of the excitation laser was 7.5 mW and the exposure time of the spectrometer was 500 ms. The repetition frequency of the Er:YAG laser was 20 Hz and the pulse energy was set

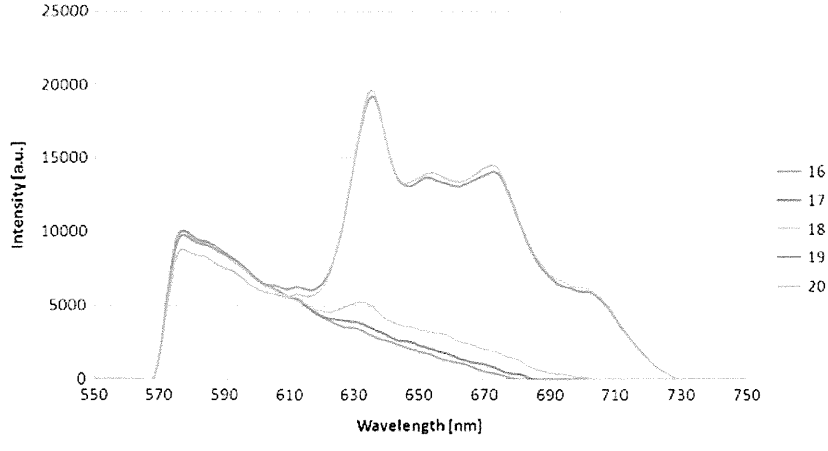

Fig. 11 Spectrum of measured five points selected from the 25 points in Fig. 10

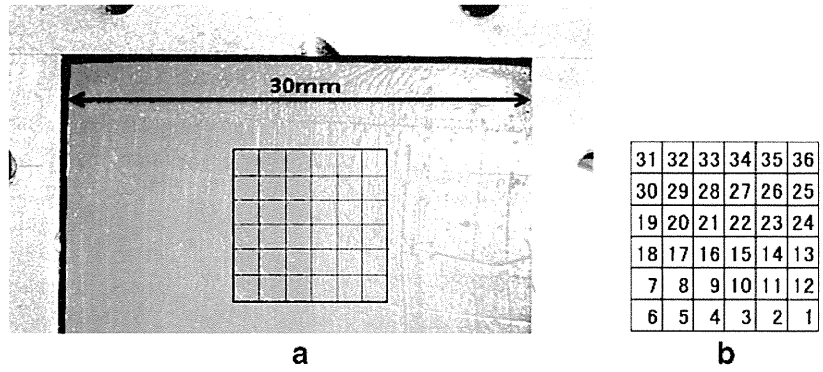

Fig. 12 Results of integrated evaluation experiment with 36 measurement points. **a** Measurement area that with received laser ablation from left-hand side; **b** corresponding measurement number

to 75 mJ/pulse. The irradiation time for each ablation was 1 s.

Figures 10 and 11 show the results of the first experiment with 25 points. Only the area containing PpIX (right-hand side of the black box) received laser ablation (Fig. 10a). However, weak fluorescence (line 18 in Fig. 11) was detected in the boundary area, which is nearest to the PpIX area. This is probably because PpIX had been excited on the border with phantom-scattered excitation light. Since the peak intensity was approximately 35 % of the region containing the PpIX, the boundary part (number 18 in Fig. 10) did not receive laser irradiation as a preparatory setting in this experiment.

Figures 12 and 13 show another set of experiment results with 36 measurement points using a different phantom (the left-hand side is filled with PpIX). The results were the same in terms of the effectiveness of the fluorescence measurement and corresponding laser ablation, even though the PpIX phantom setting is reversed. These two sets of experiments demonstrated that the system can automatically perform laser ablation by using the analyzed result of fluorescence peak intensity.

Laser ablation experiment using porcine brain tissue

We performed an in vitro experiment with a porcine brain to evaluate the effectiveness of laser ablation with angle control of the galvano mirror (Fig. 14). We assumed that the targeted area in the porcine brain is stained by PpIX. The basic principle of this laser photocoagulation for brain tissues is the use of a galvano mirror to control the direction of the co-axial excitation light and ablation laser without having to move the entire laser ablation device. Here, we also evaluated the ablation results using different laser parameters. The outputs of the Er:YAG laser used in this experiment were set to 20 Hz/75 mJ and 10 Hz/150 mJ. The irradiation time for each ablation was 1 s.

The results of porcine brain tissue irradiation are shown in Fig. 15. The diameter of each irradiation point was about 1.5 mm, and we were able to confirm that heat damage occurred around these points. The repetition frequency and pulse energy setting of 10 Hz/150 mJ showed deep irradiation and less heat damage around the irradiation hole compared with that of the 20 Hz/75 mJ setting, although the total laser power

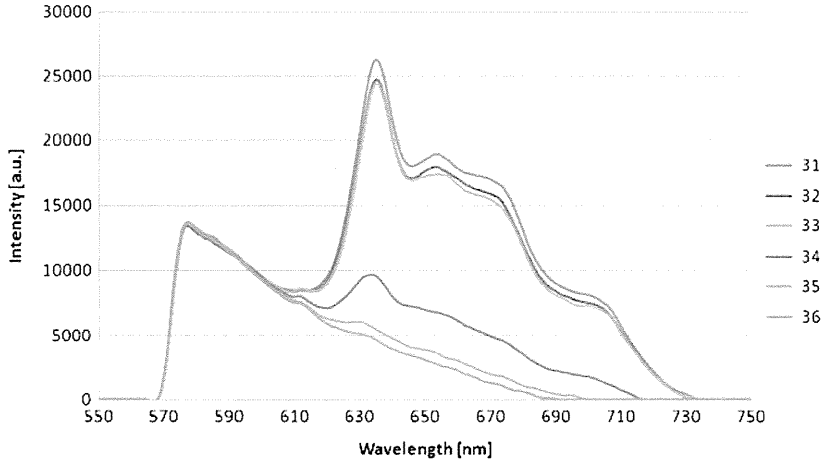

Fig. 13 Spectrum of SIX measured points selected from the 36 points in Fig. 10

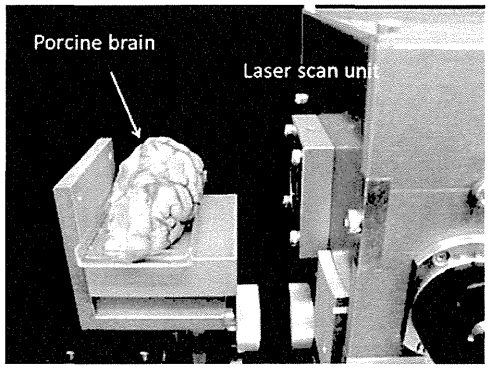

Fig. 14 In vitro experiment using porcine brain tissue

output was the same (1.5 W). The shape of the brain surface also affected the efficiency of irradiation due to corresponding changes of the laser focus point. An autofocus mechanism should be installed to achieve more precise tumor removal.

Discussion and conclusion

Overall, the experimental results showed that the proposed laser ablation system with a coaxial optical mechanism for 5-ALA fluorescence measurements and Er: YAG laser ablation could stably measure fluorescence spectra when used with a galvano scanner. The laser output was sufficient for use with brain tissue irradiation. Combination evaluations of the fluorescence measurement and laser ablation were performed on biomedical stimulant phantoms and an in vitro porcine brain.

The laser photocoagulation efficiency evaluation showed that the repetition frequency and pulse energy setting of 10 Hz/150 mJ exhibited deeper irradiation and less heat damage around the irradiation hole. Although the in vitro and biomedical stimulant phantom experiments had the same results, the optimum parameter of repetition frequency and pulse energy for laser irradiation needs to be investigated further, particularly in an in vivo environment.

In clinical cases, the boundaries between tumors and normal tissue are often unclear. A simple fluorescence peak intensity thresholding method is not well suited to treatment around the boundaries, or areas that connect with other tissues such as blood flow, or areas containing gray matter. In such areas, it is quite challenging to analyze the fluorescence data and identify the tumors. A multiple classification analysis based on other spectral features as well as the peak intensity of the fluorescence should be investigated. A fluorescence analysis system with improved measurement accuracy and a corresponding pathological comparative experiment that can better handle complicated tumor tissue structures should be included [17].

Another clinical issue that should be addressed is how to measure and perform laser ablation on the tumors located deeper and to the side. An objective lens for the laser scanning unit should be installed in the front of the unit with a set of relay lenses, designed as a rigid endoscope. We can install a mirror in the tip of such a device to reflect the laser to the side.

Our future work includes in vivo animal testing using 5-ALA-induced fluorescence measurements for the brain tissue in metabolic activity and an investigation of the laser ablation of brain tissue under the condition of blood flow and other clinical environments. Other fluorescence materials will be investigated for low-grade glioma detection to enable a wide implementation of fluorescence-guided surgery. The mechanism of the laser irradiation will be also investigated to improve the quality of tumor resection.

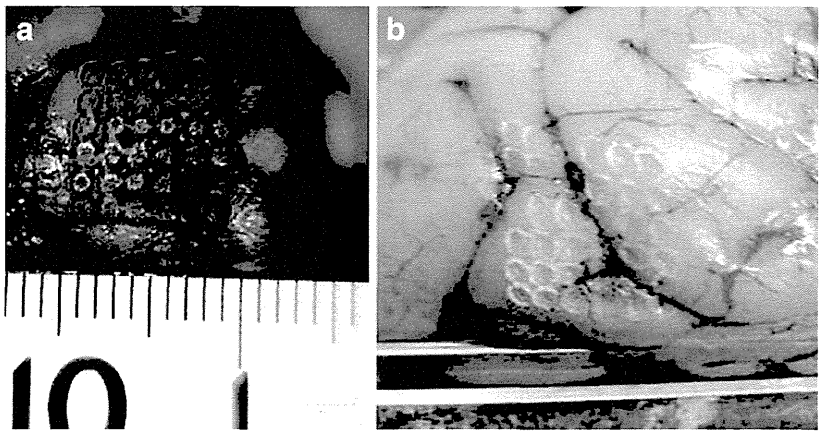

Fig. 15 Laser ablation results using porcine brain with different repetition frequency and pulse energy **a** using 20 Hz/75 mJ and **b** using 10 Hz/150 mJ

Acknowledgments This work was supported in part by Grant for Translational Systems Biology and Medicine Initiative from the Ministry of Education, Culture, Sports, Science and Technology of Japan, and Grant-in-Aid for Scientific Research (23680049, 24650289) of the Japan Society for the Promotion of Science (to Liao).

References

1. Avgeropoulos NG, Batchelor TT (1999) New treatment strategies for malignant gliomas. Oncologist 4:209–224
2. Gholipour A, Kehtarnavaz N, Briggs R, Devous M, Gopinath K (2007) Brain functional localization: a survey of image registration techniques. IEEE Trans Med Imaging 26(4):427–451
3. Liao H, Inomata T, Sakuma I, Dohi T (2010) 3-D augmented reality for MRI-guided surgery using integral videography autostereoscopic-image overlay. IEEE Trans Biomed Eng 57(6):1476–1486
4. Regula J, MacRobert AJ, Gorchein A et al (1995) Photosensitisation and photodynamic therapy of oesophageal, duodenal, and colorectal tumours using 5-aminolaevulinic acid induced protoporphyrin IX-a pilot study. Gut 36:67–75
5. Rossi FM et al (1996) In vitro studies on the potential use of 5-aminolevulinic acid mediated photodynamic therapy for gynaecological tumors. Br J Cancer 74:881–887
6. Stummer W, Stocker S, Wagner S, Stepp H, Fritsch C, Goetz C, Goetz AE, Kiefmann R, Reulen HJ (1998) Intraoperative detection of malignant gliomas by 5-aminolevulinic acid-induced porphyrin fluorescence. Neurosurgery 42:518–525
7. Stummer W, Novotny A, Stepp H, Goetz C, Bise K, Reulen HJ (2000) Fluorescence-guided resection of glioblastoma multiforme by using 5-aminolevulinic acid-induced porphyrins: a prospective study in 52 consecutive patients. J Neurosurg 93:1003–10130
8. Ciburis A, Gadonas D, Didziapetriene J, Gudinaviciene I, Grazeliene G, Kaskelyte D, Piskarskas A, Skauminas K, Smilgevicius V, Sukackaite A (2003) 5-aminolevulinic acid induced protoporphyrin IX fluorescence for detection of brain tumor cells in vivo. Exp Oncol 25(1):51–54
9. Maruyama T, Muragaki Y, Iseki H, Kubo O, Mochizuki M, Seo S, Sakuma I, Hori T, Takakura K (2001) Intraoperative detection of malignant gliomas using 5-Aminolevulinic acid induced protoporphyrin fluorescence, open MRI and real-time navigation system, computer assisted radiology and surgery. Int Congr Ser 1230:281–286
10. Leblond F, Fontaine KM, Valdes P, Ji S, Pogue BW, Hartov A, Roberts DW, Paulsen KD, (2009) Brain tumor resection guided by fluorescence imaging. In Kessel DH, (ed) Proc SPIE, volume 7164. optical methods for tumor treatment and detection: mechanisms and techniques in photodynamic therapy XVIII
11. Omori S, Muragaki Y, Sakuma I, Iseki H (2004) Robotic laser surgery with λ=2.8 μm microlaser in neurosurgery. J Robtics Mechatron 16(2):122–128
12. Nakajima A, Iwami H, Nishimura M, Muragaki Y, Iseki H (2008) Development of Re:YAG laser surgery system for neurosurgery. J JSCAS 10(1):19–27
13. Yamanaka N, Yamashita H, Masamune K, Liao H, Chiba T, Dohi T (2009) A coaxial laser endoscope with arbitrary spots in endoscopic view for fetal surgery, 12th International Conference on Medical Image Computing and Computer-Assisted Intervention–MICCAI 2009. Lect Notes Comput Sci LNCS 5761:83–90
14. Noguchi M, Aoki E, Yoshida D et al (2006) A novel robotic laser ablation system for precision neurosurgery with intraoperative 5-ala-induced PpIX fluorescence detection. 9th International Conference on Medical Image Computing and Computer-Assisted Intervention—MICCAI 2006. Lect Notes Comput Sci LNCS 4190:543–550
15. Liao H, Shimaya K, Wang K, Maruyama T, Noguchi M, Muragaki Y, Kobayashi E, Iseki H, Sakuma I (2008) Combination of intraoperative 5-aminolevulinic acid induced fluorescence and 3-D MR imaging for guidance of robotic laser ablation precision neurosurgery, 11th International Conference on Medical Image Computing and Computer-Assisted Intervention—MICCAI 2008. Lect Notes Comput Sci 5242:373–380
16. Liao H, Noguchi M, Maruyama T, Muragaki Y, Kobayashi E, Iseki H, Sakuma I (2012) An integrated diagnosis and therapeutic system using intraoperative 5-aminolevulinic-acid-induced fluorescence guided robotic laser ablation for precision neurosurgery. Med Image Anal 16(3):754–766
17. Ando T, Kobayashi E, Liao H, Maruyama T, Muragaki Y, Iseki H, Kubo O, Sakuma I (2011) Precise comparison of protoporphyrin IX fluorescence spectra with pathological results for brain tumor identification. Brain Tumor Pathol 28(1):43–51

Medical Image Analysis 16 (2012) 754–766

Contents lists available at ScienceDirect

Medical Image Analysis

journal homepage: www.elsevier.com/locate/media

An integrated diagnosis and therapeutic system using intra-operative 5-aminolevulinic-acid-induced fluorescence guided robotic laser ablation for precision neurosurgery

Hongen Liao [a,b,*], Masafumi Noguchi [c], Takashi Maruyama [d], Yoshihiro Muragaki [d], Etsuko Kobayashi [c], Hiroshi Iseki [d], Ichiro Sakuma [b,c]

[a] Department of Bioengineering, Graduate School of Engineering, The University of Tokyo, Tokyo, Japan
[b] Translational Systems Biology and Medicine Initiative, The University of Tokyo, Tokyo, Japan
[c] Department of Precision Engineering, Graduate School of Engineering, The University of Tokyo, Tokyo, Japan
[d] Graduate School of Medicine, Tokyo Women's Medical University, Tokyo, Japan

ARTICLE INFO

Article history:
Received 5 September 2009
Received in revised form 30 September 2010
Accepted 8 November 2010
Available online 28 November 2010

Keywords:
Neurosurgery
5-Aminolevulinic-acid
Fluorescence
Integrated diagnosis and therapeutic system
Medical robotics

ABSTRACT

We have developed an integrated diagnosis and therapeutic system for precision malignant gliomas resection during neurosurgery. A combination of three-dimensional (3-D) magnetic resonance imaging (MRI) navigation and 5-aminolevulinic acid (5-ALA)-induced fluorescence based intra-operative tumor diagnosis technique has been incorporated into a robotic laser ablation neurosurgery system with an automatic focusing and robotic scanning mechanism. 5-ALA is a non-fluorescent prodrug that leads to intracellular accumulation of fluorescent protoporphyrins IX (PpIX) in malignant glioma. The PpIX tends to accumulate in pathological lesions, and emits red fluorescence when excited by blue light. This fluorescence is illuminated with laser excitation, enables intra-operative identification of the position of a tumor and provides guidance for resection with laser photocoagulation. The information provided by the MRI is enhanced by the intra-operative 5-ALA fluorescence data, and this enhanced information is integrated into a robotic laser ablation system. The accuracy of the fluorescent measurement of the tumor is improved using high-precision spectral analysis. The fluorescence assists in the detection of malignant brain tumors intra-operatively and improves their removal rate.

1. Introduction

Malignant gliomas are the most common primary brain tumor, and victims have poor prognosis even after treatment with a combination of surgery, chemotherapy, and radiotherapy. Among the factors determining the prognosis in malignant gliomas treatment, the extent of the resection remains controversial because malignant gliomas cannot be completely resected using conventional surgical techniques. During tumor ablation surgery, the surgeon needs to identify the edges of the tumor in order to perform a complete tumor resection. Surgeons can resect most tumors with an accuracy of millimeters using a combination of conventional surgical instruments and a computer-aided navigation system with diagnostic images, such as magnetic resonance (MR) and computed tomography (CT) images. However, regardless of the extent of the surgery, some tumor cells remain in the areas adjacent to the tumor removal area because of the uncertainty involved in indentifying viable tumor margins during surgery. These residual cells, especially those of malignant tumors like glioma, impair the prognosis of the patient. It is necessary to resect the tumor completely while preserving as much normal tissue as possible.

During neurosurgery, cerebrospinal fluid leakage and surgical interventions deform the brain tissue. This so-called "brain shift" can be as much as several tens of millimeters and continues to increase during the surgical procedure (Clatz et al., 2005). There is thus a strong need for accurate and precise image-guided surgical navigation based on intra-operative imaging. However, image-guided navigation can be off by as much as a few millimeters due to inaccurate registration of the pre-operative diagnostic images and intra-operative images (Gholipour et al., 2007; Liao et al., 2006). Although intra-operative imaging is only rarely available, the use of intra-operative imaging such as ultrasound enables more accurate diagnosis for treatment. In neurosurgery treatment, ultrasound images can also assist in the identification of the target and critic areas in real time during neurosurgical treatment (Unsgaard et al., 2006; Sosna et al., 2005). Furthermore, there is a tradeoff between more frequent image acquisition for more accurate navigation and less frequent acquisition for computer resource conservation.

* Corresponding author at: Hongen Liao, 7-3-1 Hongo, Bunkyo-ku, Tokyo 113-8656, Japan. Tel.: +81 3 5841 6461; fax: +81 3 5841 7915.
E-mail address: liao@bmpe.t.u-tokyo.ac.jp (H. Liao).

1361-8415/$ - see front matter © 2010 Elsevier B.V. All rights reserved.
doi:10.1016/j.media.2010.11.004

Several advanced surgical tools and imaging techniques have been developed and are becoming widely used to guide surgeons in tumor resection. The use of open magnetic resonance imaging (MRI) devices enables the intra-operative identification of remaining tumor tissue during the operation (Hirai et al., 2005). However, due to the difficulty in delineating the boundary between tumor tissue and nontumorous tissue, it is not easy to resect the entire tumor with MRI guidance, especially for tissue near functional areas of the brain. In neurosurgery, since distinguishing tumor tissue from normal brain tissue under white light during neurosurgery is difficult, finding a way to provide intra-operative imaging for small tumors or residual tumor tissue is a major challenge.

Electrocortical and subcortical stimulation, for example, can aid in identification of functional regions in real time during intervention (Suess et al., 2006; Pouratian et al., 2004; Keles et al., 2004). Intra-operative electrocortical and subcortical stimulation mapping are regarded as a useful standard of intra-operative mapping for predicting functional outcomes although they have several disadvantages and are quite demanding techniques. Functional MRI (Ogawa et al., 1990) and magnetoencephalography (MEG) (Cohen, 1968), two of the most recently developed forms of neuro-imaging, are helpful in delineating the eloquent areas of the brain by means of functional brain mapping (Muragaki et al., 2001; Fukaya et al., 2002; Hashizume et al., 2007). Although a combination of such techniques can provide high spatial and temporal resolution, real-time information acquisition is still a challenge.

One technique is to illuminate the brain tumor tissue with 5-aminolevulinic acid (5-ALA)-induced protoporphyrin IX (PpIX) fluorescence (Regula et al., 1995). The use of 5-ALA for intra-operative visualization of malignant glioma tissue enables greater completeness of tumor removal (Ciburis et al., 2003). This acid is a natural biochemical precursor of hemoglobin that elicits synthesis and accumulation of fluorescent porphyrins in various epithelia and cancerous tissue. In neurosurgery, surgeons wear a modified neurosurgical microscope and use blue-violet light to see the fluorescent tissue. The fluorescence is used to identify residual malignant glioma intra-operatively so that the surgeon can improve the accuracy of surgical treatment (Rossi et al., 1996; Stummer et al., 1998b; Stummer et al., 2000). Previous reports on 5-ALA guided neurosurgery focused on the necessary modifications to components of the neurosurgical microscope for fluorescence-guided micro-surgical resection of malignant gliomas (Maruyama et al., 2001; Stummer et al., 1998a). With the illumination of 5-ALA-induced fluorescence in microscopic surgery, a surgeon can resect the tumor more accurately (Leblond et al., 2009; Valdes et al., 2009). However, to achieve 100% resection of tumor tissue safely and precisely, both positioning accuracy in diagnosis and tumor ablation accuracy in treatment are required.

Treatment for malignant gliomas depends on the location, cell type and grade of the malignancy. Usually, the treatment is a combined approach using surgery, radiation therapy, and chemotherapy. Although microscope-based surgery provides an accuracy of several mm to several sub mm, the level achieved depends on the skill of the surgeon. A non-contact therapeutic approach is a good way to improve ablation accuracy because conventional surgery tends to deform the brain. An example of such an approach is laser photocoagulation under the guidance of an MRI navigation system (Omori et al., 2004).

The aim of our research project is to develop a system that integrates automatic tumor identification using intra-operative fluorescence with accurate tumor treatment using precise robotic laser ablation. To improve treatment accuracy, we developed a diagnosis and therapeutic system that combines 5-ALA fluorescence-enhanced intra-operative navigation with a micro-laser ablation device (Liao et al., 2008; Noguchi et al., 2006). The boundary between tumorous and nontumorous tissue is identified using 5-ALA-induced PpIX fluorescence, and the tumor is accurately ablated with the micro-laser. The combination of 5-ALA fluorescence guidance and high-precision spectral analysis enables higher tumor identification accuracy than with a system that uses only pre-/intra-operative MR imaging. A laser manipulation system based on robotic technology guides the laser beam onto the lesion, resulting in tumor ablation with sub mm accuracy. The performance of the laser and positioning system was evaluated using a set of phantom experiments and a dissected porcine brain.

2. Materials and methods

2.1. Intra-operative identification of brain tumors using 5-ALA

5-ALA is the first compound in the porphyrin synthesis pathway, which leads to hemoglobin in mammals and chlorophyll in plants. As a metabolic precursor in the haem biosynthesis pathway, 5-ALA elicits synthesis and induces the synthesis of PpIX and other porphyrins with fluorescing and photosensitizing properties not only in malignant gliomas but also in malignancies of other organ systems. Since 5-ALA leads to accumulation of fluorescent porphyrins in malignant glioma tissue, the gliomas can be detected using 5-ALA-induced porphyrin fluorescence. The fluorescence enables better detection of tumorous tissue and improved tumor resection during neurosurgical procedures. Studies have shown that the intra-operative use of this guiding method may also reduce the residual tumor volume and prolong progression-free survival in patients suffering malignant glioma (Stummer et al., 2000).

Before fluorescence-guided surgery, the patient drinks a glass of water in which 5-ALA has been dissolved. The 5-ALA turns into PpIX when it is ingested by a living organism. The PpIX tends to accumulate in pathological lesions, so when it is excited by blue-violet light, any brain tumors are easy to spot due to the PpIX emitting red fluorescence (Fig. 1b). Compared with the image of the tumor captured under white light (Fig. 1a), the tumor regions can be easily recognized by the surgeon. They can thus be identified and then resected with a microscope equipped for fluorescence-guided surgery.

2.2. Spectra analysis of 5-ALA-induced fluorescence for malignant glioma

During fluorescence detection, the tumor is illuminated by a guide laser diode (405 ± 5 nm; Digital Stream Co., Ltd., Kanagawa) connected to an incoherent light system emitting blue-violet light. The laser beam diameter is 1 mm; the output is set to 0.7 mW to reduce photobleaching of surrounding areas. The fluorescence is collected by a detection probe and guided into a spectrometer through an optical multi-mode fiber and then into a PC for spectral analysis (Fig. 2a). Spectra of brain tissues are acquired in-vivo and optical filters are selected through simulation using these spectra. In addition, a method is developed for detecting tumor regions using a two-dimensional histogram acquired from two intensity images. The system is evaluated through fluorescent measurement of brain tissues in-vivo, and the measurement results are compared with the simulation results. Furthermore, the regions in which the fluorescent properties are uniform are identified by analyzing the image intensity of the fluorescence. We divide the observed tissues into "tumor", "non-tumor" and "blended boundary" using the spectral analysis results.

A detection probe is designed and used to assess the use of fluorescence in identifying malignant glioma after administration of 5-ALA for collecting PpIX fluorescence (Fig. 2b). The fluorescence is transferred to a spectrophotometer through an optical single-mode fiber (Fig. 2c) for spectral analysis. We also develop a measurement

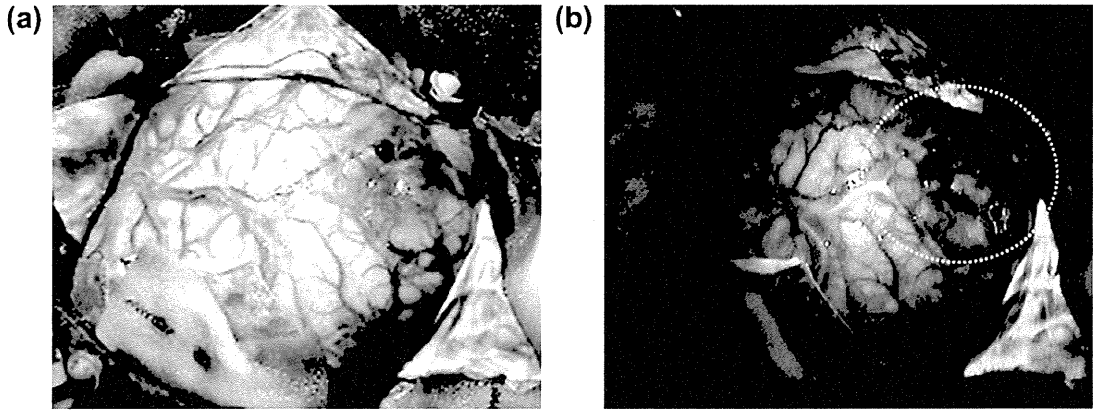

Fig. 1. Detection of tumor using 5-ALA-induced fluorescence illumination: (a) Image captured under white light; (b) image captured under 5-ALA-induced fluorescence (red areas in circle).

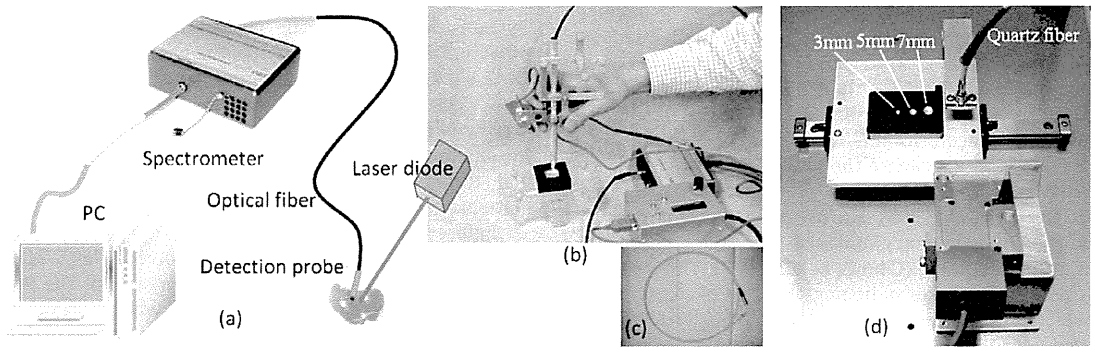

Fig. 2. (a) Optics setting and 5-ALA-induced protoporphyrin IX (PpIX) fluorescence spectral analysis system. (b) Prototype for spectral analysis of 5-ALA-induced PpIX fluorescence. (c) Probe for spectral measurement. (d) Measurement device for pathological analysis of clinical samples.

device with dishes to hold tissue of clinical samples for pathological analysis (Fig. 2d). The dish has a different diameter of 3, 5, or 7 mm, and aspheric lenses are used to correct for aberrations. The detection resolution is set to 0.6 mm in consideration of the tradeoff between the acquired light intensity (which is in proportional to the square of the detection diameter) and measurement accuracy. A band-pass filter (over 60% transmission at 635 nm and up to 5% at 670 nm) is fixed to the tip of the detector. The filter cut off the excitation light and the guide laser light (peak at 670 nm).

Fig. 3a shows the spectra for 5-ALA-induced PpIX fluorescence with characteristic peaks at 635 and 704 nm in the tumor region, and Fig. 3b shows the spectra for the non-tumor region. The spectra of the tumor tissue and the non-tumor tissue are easy to be discriminated, while the spectra discrimination of blended boundary with both tumor and non-tumor tissues are difficult (Fig. 3c).

We also evaluated the characteristic spectra of tumors by comparing them with pathological analysis results (Ando et al., 2009). A local spectrum measurement system for 5-ALA-induced PpIX fluorescence was developed, and a set of clinical statistics data was used to evaluate the system. The spectra for 754 points from 13 samples (including glioblastoma multiform, anaplastic oligodendroglioma, anaplastic oligodendro-astrocytoma and oligodendroglioma) were acquired and analyzed. The analysis results showed that both the PpIX fluorescence and the intensity were distributed, and the intensity distribution of PpIX fluorescence acquired by the developed system was similar to that of the PpIX intensity of a tumor. Experiments comparing the local spectrum of protoporphyrin IX fluorescence with pathology showed a good relationship between the spectra and the pathological results. The accuracy of tumor identification could be improved by dedicated analysis of tissue samples.

Holding the probe manually during microscopic surgery means that the procedure must be interrupted to move the surgical microscope out of the way in order to assess the tumor fluorescence, and then the microscope must be returned to its original position in order to continue the procedure. To overcome this problem, we mount the probe on a robotic manipulator which eliminates the need to interrupt the procedure to assess the fluorescence as described in Section 2.4.

2.3. MR imaging navigation for rough identification of tumor areas

Removing malignant glioma completely in neurosurgery is a complicated task. Obscure boundaries between normal and abnormal tissues prevent the surgeon from identifying the edges of the glioma accurately. MRI-based navigation helps surgeons to identify the entire tumor in a clinical implementation. An open-MRI device is used to obtain intra-operative information that can be used to compensate for brain deformation that occurs during the procedure. The intra-operative information acquired by various surgical measurement systems must be integrated for effective surgical navigation.

Pre- and intra-operative MR imaging are used to identify the area of the tumor roughly. The MR imaging navigation system is registered using a POLARIS optical tracking device (Northern Digital

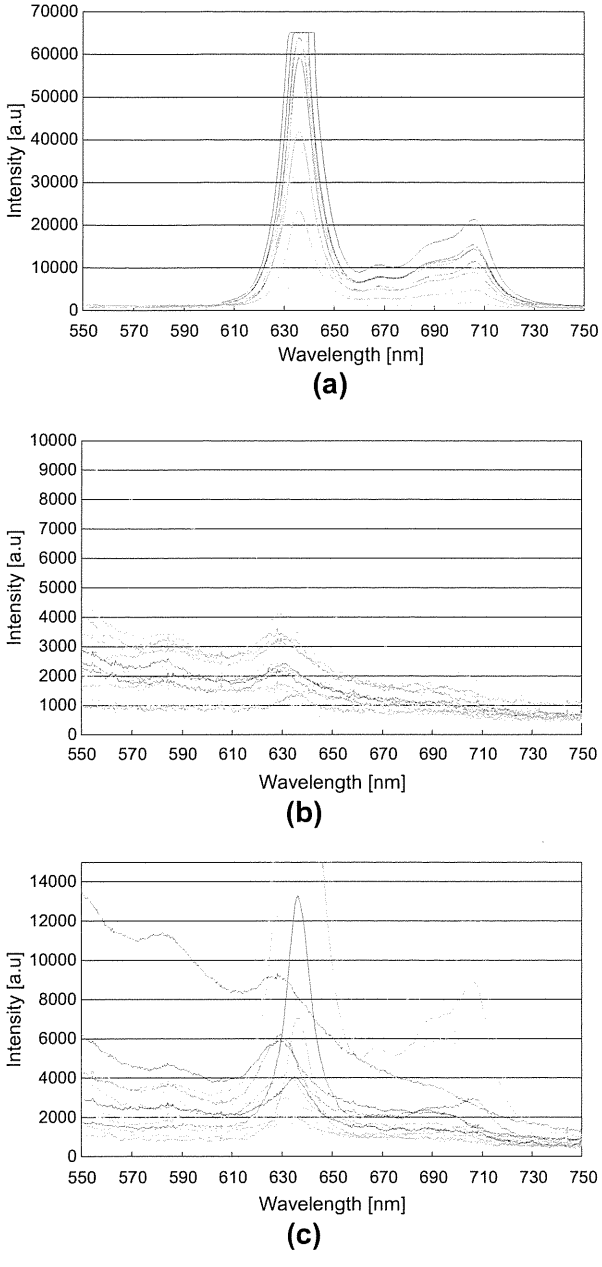

Fig. 3. Spectra analysis of 5-ALA-induced protoporphyrin IX (PpIX). Each line represents a sample. (a) Spectra for tumor tissue with characteristic peaks at 635 and 704 nm. (b) Spectra for non-tumor tissue. (c) Spectra for blended boundary with both tumor and non-tumor tissues.

Inc., Canada). During the operation, the distance between the ablation laser and tumor can be adjusted using the automatic focusing (AF) system, which is fixed to the fluorescence spectra acquirement devices as described in the next section. These devices are attached by anther optical tracking probe, which can be tracked by the same optical tracking device. Patient-image registration can be based on a set of distinct features such as geometrical landmarks or natural anatomical landmarks that can be accurately identified in both spaces. The fiducial markers used in image registration provide pairs of corresponding 3-D points in the spaces to be registered. Once the coordinates of the fiducials in the information space and in the patient coordinate space have been determined, the geometric transformation that associates these two spaces can be derived. In this study, a set of MR markers was attached the patient's body, enabling us to calculate the transformation matrix between the original devices and then calculate the relationship between the patient's body and the navigation system.

Since brain shift leads to large errors with pre-operative or even intra-operative MR imaging, high precision intra-operative information must be integrated into the MRI navigation system after finishing rough patient-image registration. The intra-operative measurement with 5-ALA-induced fluorescence can be integrated into the MR imaging navigation to obtain higher positioning precision of the entire or the residual tumor during the operation. The boundary identified by the fluorescence can be used to correct for errors between the MR imaging and the patient's body. Thus, the information provided by the MRI navigation system is enhanced by the addition of fluorescence data. The navigation system is integrated with the robotic manipulation system for laser scanning and laser ablation. This combined system can provide an intra-operative overview of both the information about the tumor surface obtained by fluorescence and the 3-D structure of the tumor obtained by MRI. The 5-ALA-induced fluorescent-guided system provides high-precision identification of the tumor surface while MRI navigation provides information about the entire structure of the tumor, especially in the depth direction.

For large area guidance, an intra-operative MR image can also be used to identify the tumor in the rough, especially the 3D shape of the tumor. The fluorescence is used to precisely indentify small tumors or residual tumor tissue during an operation and provides guidance for laser ablation. After the surface of the resected areas is cleared, the fluorescence continues to provide information about the tumor as long as there is any residual tumor tissue. Actually, the fluorescence gives information about the surface layer of the tumor. The fluorescence can be used to identify the boundary area of gliomas and small tumors that are difficult to distinguish from normal brain tissue under white light.

2.4. Fluorescence scanning and laser photocoagulation device with automatic focusing mechanism

The laser scanning and tumor ablation procedure includes three steps: (1) scan the tumor and measure the spectra of the fluorescence; (2) segment the analyzed fluorescence area and identify the tumors; (3) perform laser ablation on the target. The configuration of the laser photocoagulation and manipulation system is shown in Fig. 4 and the prototype is shown in Fig. 5.

First, the operator defines the measurement area roughly in a charge coupled device (CCD) camera view of the AF system with guidance from MRI navigation, as described in Section 2.3. The area is sectioned into a grid pattern with a grid interval of 0.2 mm. Measurement is performed at the central point in each grid square using step scanning. The test of each square, 0.2 mm on a side, is regarded to have the same fluorescent properties as the measurement point. As the measurement at each point requires more than a few hundred milliseconds for integration of the spectral photometer, the measurement takes 10 s to cover a mm^2.

Second, the system segments the fluorescent area and saves the coordination data of the grid. The fluorescence intensity is calculated from the spectral data, and binarization is performed using Otsu's thresholding method (Otsu, 1979). After the system finishes identifying the fluorescence area corresponding to the tumor, the micro ablation laser uses automatic scanning to ablate the area. The ablation speed is 1 mm/s, and the pitch is 0.1 mm.

The precision of the laser ablation is due to combining the positioning precision of the AF system with the precision of the laser ablation. It is necessary to keep the distance between both the

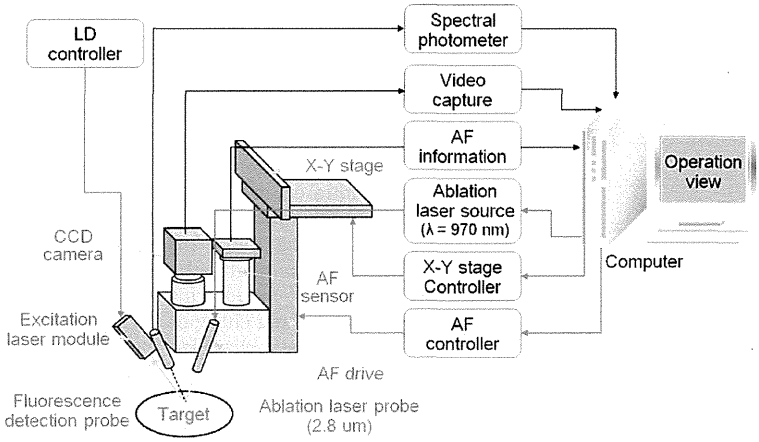

Fig. 4. Overview of system combining tumor detection using 5-ALA-induced PpIX fluorescence tumor detection system and precise ablation with a micro-laser with an automatic focusing and robotic scanning mechanism.

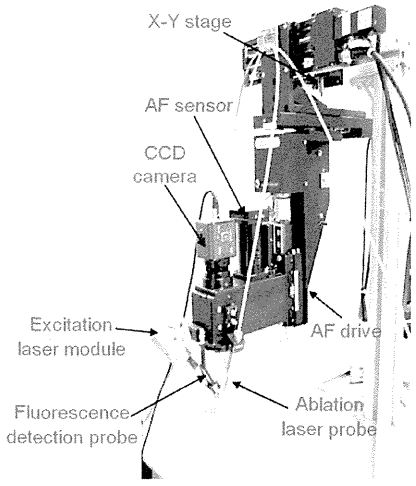

Fig. 5. Prototype of fluorescence scanning and laser photocoagulation device with automatic focusing mechanism.

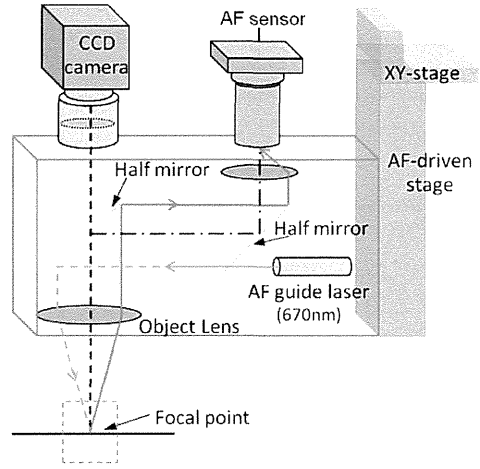

Fig. 6. Non-contact surface profiling system with automatic focusing and scanning mechanism.

CCD camera and laser head and the ablation area at a given level. Both the fluorescence detection probe and the micro-laser probe have an appropriate working distance from the target surface, so the AF mechanism must constantly maintain the appropriate distance. Before using these probes, we calibrated them to intersect at the same focusing point. The auto-focus mechanism along with reference laser measurement was used to track the distance between the target and ablation device. We used the scanning system to scan the target to obtain the corresponding spatial position of the target surface. The working distance could then be adjusted automatically in accordance with the measurement results.

The AF system was designed on basis of a three-dimensional position measurement system. Position measurement is performed using a confocal optical mechanism that combines a guide laser and a split photodiode, enabling focusing with an accuracy of micrometers. This system is coupled with a two-axial (XY) automatic stepping drive stage that can perform a robotic scanning on the brain surface. The principle of this mechanism and the control for the AF measurement system are illustrated in Fig. 6. The object lens is mounted on a linear scale, which can be moved around the *Z*-axis. A guide laser is installed inside the AF mechanism and carried out through an offset lens in the optic axis. The reflected laser light is made to create an image on a two-division-type photodiode (AF sensor). The laser beam is illuminated with an offset to the optical axis of the objective lens. The laser light reflecting on the target surface is collected with a co-axial optical system and guided to photodiode (Fig. 7a). The light spot is positioned to derive the displacement. The laser spot image hits in the center of the AF sensor when it is adjusted to the focusing point while the spot position is displaced right and left at the time of defocusing (Fig. 7b), which requires feedback on the differential output of the sensor to the AF drive mechanism. The AF system adjusts the distance between the lens and target accordingly. A CCD camera optical system is included in the coaxial system, and the object can be observed due to the co-focus.

The AF mechanism enables automatic adjustment of the distance between the camera and the brain surface to keep the focus point of the fluorescence scanning and laser ablation devices at the required position. The peak wavelength of the guide laser for the AF system is 670 nm. The surgical field view can be observed through a CCD camera coaxially incorporated in the AF system. We used a laser displacement meter (LB-62/LB-02, Keyence Co., Ltd., Japan) to measure the movement of the AF mechanism. The scanning and AF servo-mechanisms had a precision of 10 μm.

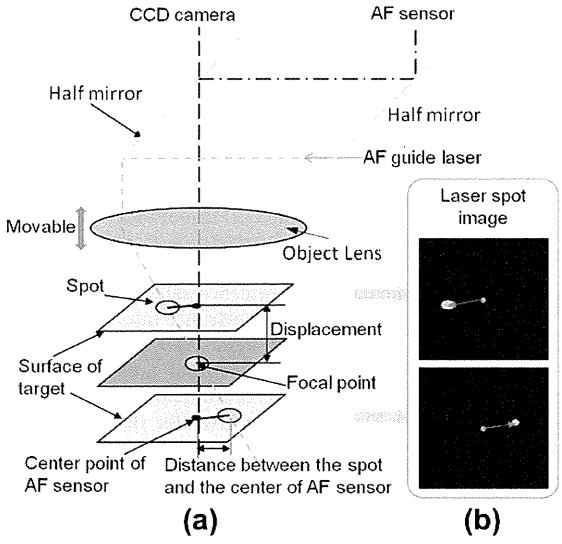

Fig. 7. Automatic focusing mechanism. (a) Laser light reflecting on the target surface is collected with a co-axial optical system and guided to photodiode (AF sensor); (b) laser spot images captured by AF sensor with spot positions displaced right and left at the time of defocusing.

The focusing range of the AF system was evaluated by measuring how much the defocusing of the system can be shifted from its focal position (Liao et al., 2010). A repetition test for evaluation of the performance of the AF mechanism was also conducted. Focusing accuracy is within ±0.5 mm relative to the movement of the brain surface caused by pulsation and respiration.

2.5. Micro ablation laser module

We use an infrared continuous-wave laser with a wavelength of 2.8 μm. The beam is output by a microchip solid-state laser on the tip of the micro-laser probe. The pumping light source for the laser is a near-infrared laser diode with a wavelength of 970 nm, and the light is guided through a quartz optical fiber to the laser probe.

Since light with a wavelength around 3 μm is strongly absorbed by water, the laser is effective only on the surface of living tissue. Furthermore, the laser can perform a precise ablation at low output (0.5 W or less). The laser beam is focused to a diameter of 0.1–0.15 mm with a lens, and an ablation groove is formed equivalent to the spot diameter in the soft tissue. The working distance of the laser probe is 20 ± 1 mm.

2.6. System integration

As described above, our laser ablation system includes a 5-ALA-induced PpIX fluorescence tumor detector, a micro-laser module, an MR imaging navigation system, and an automatic focusing and robotic scanning system. The fluorescence detection probe and micro-laser probe are attached to the AF system. As shown in Fig. 8, the data from the spectral photometer is analyzed using a PC. The analyzed results are used for assisting intra-operative detection of the brain tumor and its boundaries. Switching between micro-lasing and scanning with the step-driven stage is controlled by the PC. The prototype is characterized by positioning of the irradiation beam by observing the target using a CCD camera and by ablation of the lesion surface by evaporation etching. An automatic stage mechanism is positioned on a plane perpendicular to the AF axis and used to determine the spatial position of the brain surface. We perform laser scanning from one side to the other. The AF guided fluorescence detection system records the information for the scanned area, both the fluorescence spectra and 3D position information.

The navigation system is used to control electric motors that position the fluorescence measurement and laser ablation instruments. Since the intra-operative information of the surgical area is displayed in this system, the surgeon can treat the entire tumor. The micro-laser is effective only on the surface of brain tissue, enabling precise ablation at the boundary between the tumor and normal tissue.

3. Experiments and results

We combined MR imaging and 5-ALA-induced PpIX fluorescence in the tumor detection system, and integrated the system with a

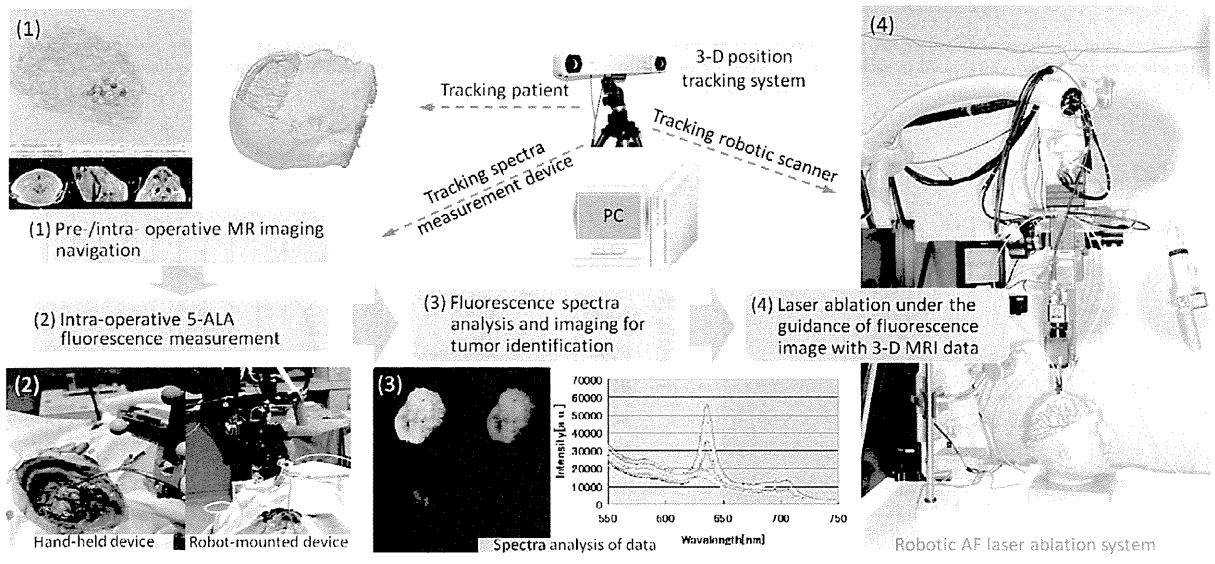

Fig. 8. System configuration of laser ablation treatment with guidance of 5-ALA-enhanced intra-operative navigation.

micro ablation laser module for treatment. We conducted a set of combination experiments to evaluate the system using a biomedical stimulant material (phantoms) and a porcine brain. Our first experiment was to discriminate the fluorescence intensity threshold and fluorescent region. The subsequent set of experiments was used to discriminate the PpIX regions and to determine the distribution of fluorescence intensity (Section 3.1). The method used for threshold discrimination and the experimental results used for in-vivo testing of the spectra measurement and analysis are described in Section 3.2. After this fluorescence spectral analysis, the system was evaluated to determine whether it can delineate the spatial boundary between an area with fluorescence and one without it with the guidance of MRI and fluorescence, as described in Section 3.3. We also integrated MRI-guided tumor identification with fluorescence to validate system implementation, as described in Section 3.4. Finally, we conducted an animal experiment to evaluate the system for fluorescence identification and laser ablation.

3.1. Discrimination for fluorescence intensity threshold and fluorescent region

The first experiment was to discriminate the fluorescence intensity threshold and fluorescent region. We manufactured an agar plate containing Intralipid-10% as an optical simulant material for brain tissue (Fig. 9a). The concentration of Intralipid-10% was set so that the scattering coefficient (us1) was 3 cm^{-1} in the PpIX area and 30 cm^{-1} in the other area, values similar to those of glioma and white matter (Staveren et al., 1991; Sterenborg et al., 1989). The phantom surface was inclined at an angle of 8° to the x-axis of the system. The integration time for spectral measurements was 300 ms.

Fig. 9 illustrates the fluorescence measurement procedure. First, the measurement area is set in the CCD camera view (Fig. 9a). The area is then sectioned into a grid pattern, and spectral measurement is performed at the central point in each grid (Fig. 9b). Fig. 9c shows the calculated fluorescence intensity and discriminated parts of the PpIX area. The fluorescence intensity was calculated from the spectral data, and an intensity level was determined as a threshold for distinguishing the tumor areas. As shown in Fig. 10, the two areas (fluorescent area from non-fluorescent) were clearly distinguished. The extraction error for the true boundary line was less than 0.1 mm (Fig. 10b).

We conducted another set of experiments to perform discrimination of PpIX regions and distribution of the fluorescence intensity (Fig. 11). The underlying clinical hypothesis of this experiment was to identify the boundary area for separated tumors with different sizes and to evaluate the accuracy of the fluorescence identification. Three different patterns with PpIX in agar plates

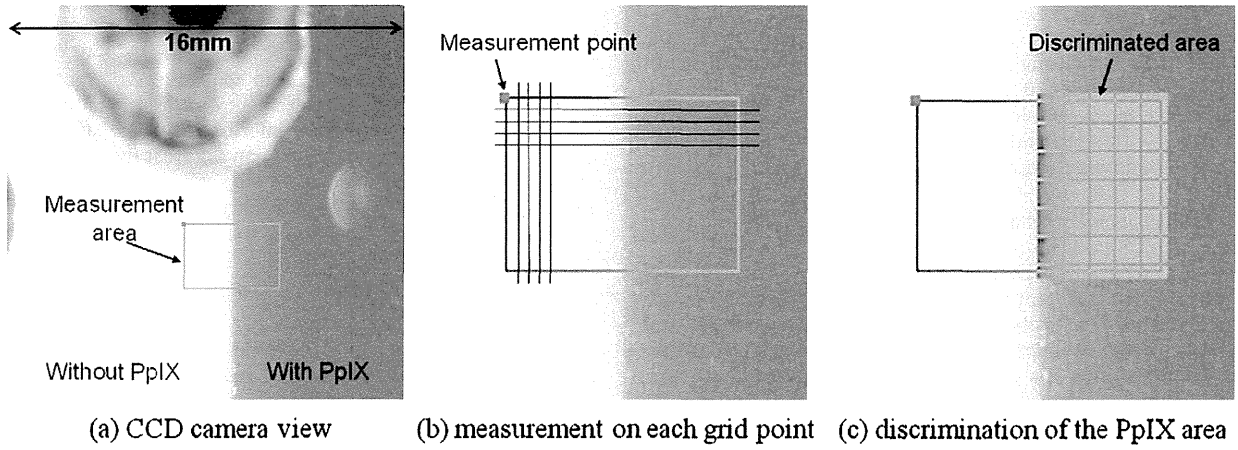

Fig. 9. Illustration of fluorescence measurement procedure of: (a) Measurement area is set in CCD camera view; (b) area is sectioned into grid pattern and spectral measurement is performed at central point in each square; (c) fluorescence intensity is calculated, and PpIX area is discriminated using thresholding method. Red square represents fixed reference point.

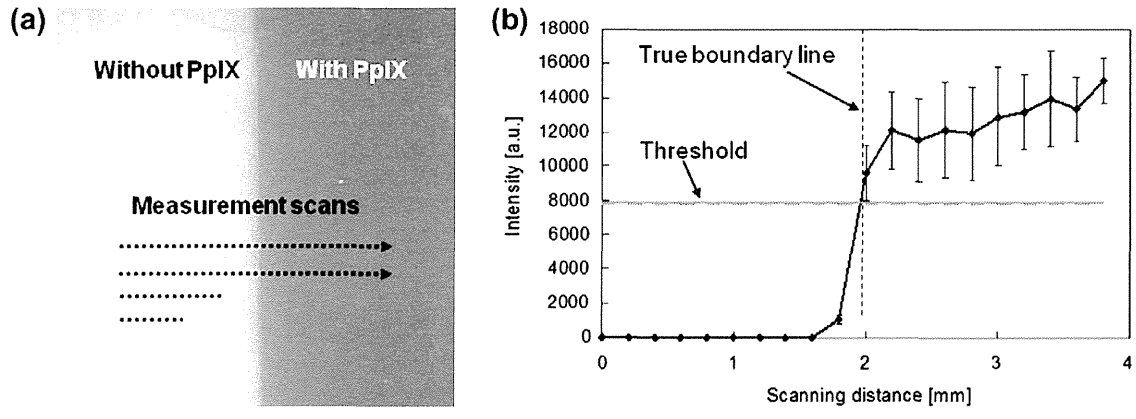

Fig. 10. Measurement of fluorescence intensity: (a) Agar plate divided into areas with and without PpIX; (b) discrimination results for fluorescence intensity threshold.

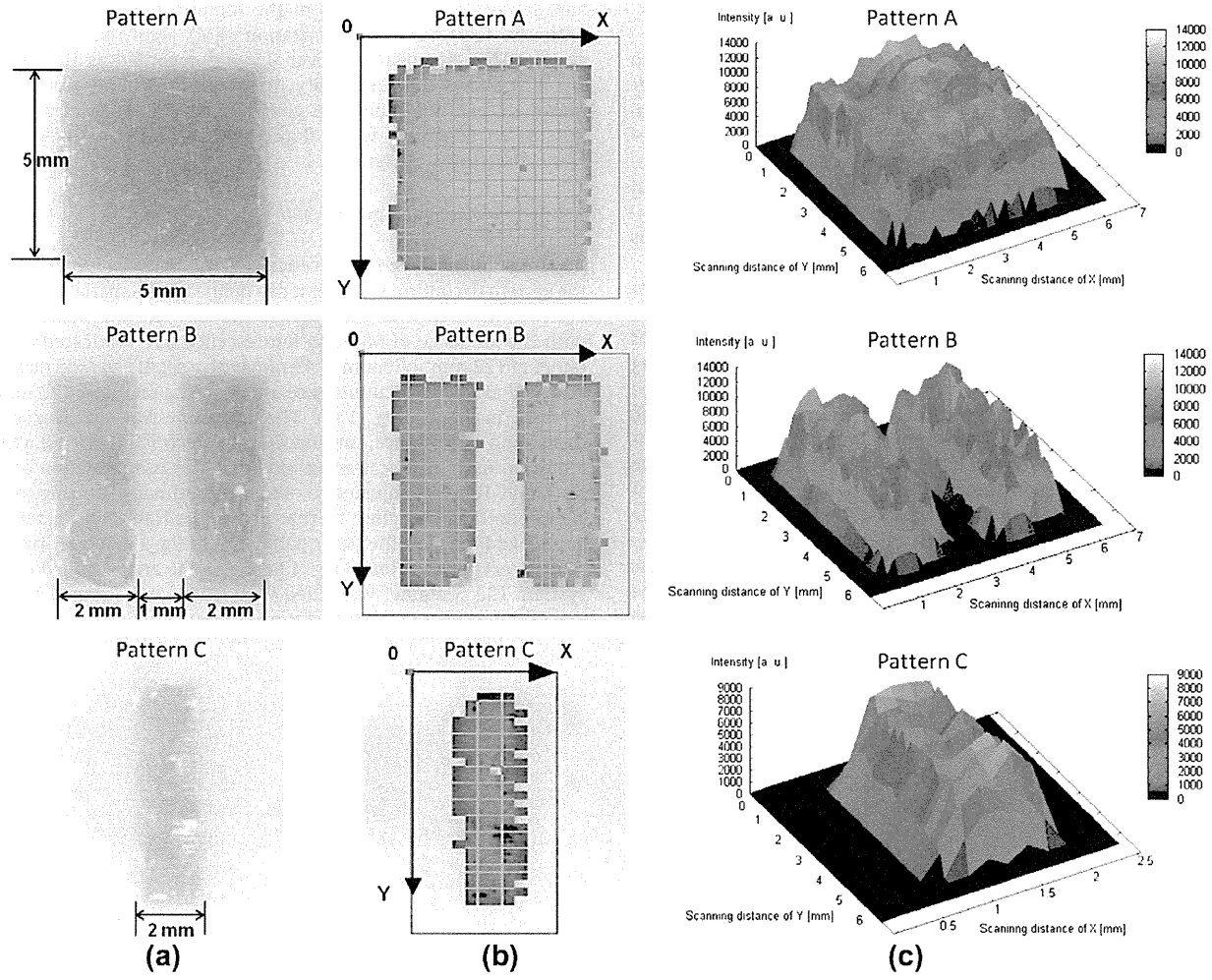

Fig. 11. Three different patterns (upper, middle, and lower) with PpIX in agar plates for simulating optical property of brain tissue with different sizes: (a) Pattern with PpIX in agar plate. (b) Discrimination for PpIX regions. (c) Distribution of fluorescence intensity.

were manufactured (Fig. 11a). Fluorescence intensity was achieved only on the PpIX area and its neighborhood. Discrimination error at boundary lines and accuracy rate of the extraction inside the fluorescent region is in Table 1. Discrimination error was determined from the distance between the discriminated area and the true boundary line. Significant different was not observed in discrimination accuracy along three patterns. Distributions of the fluorescence intensity and the results of segmentation are shown in Fig. 11c.

The phantoms used in the preliminary experiments included only a single fluorescent species, PpIX. These experiments, based on the threshold technique, were used to identify the feasibility of discriminating fluorescent and non-fluorescent areas. Although these experiments using phantoms enabled precise measurement and discrimination, only fluorescent and non-fluorescent areas were simulated. Moreover, the optical parameters of the Intralipid-10%, such as its absorption and scattering properties, affected the simulation results. Due to the complex nature of biological tissue, the effect of the environment surrounding a particular fluorophore and its background information should also be considered. For example, there is a wide variety of endogenous fluorophores, an autofluorescent species, in biological tissue. Some of the intense endogenous fluorophores in human tissue are involved in cellular metabolism (Vo-Dinh, 2003). In this case, the concentration of fluorophores should be controlled so that the optical phantoms have the same absorption and scattering coefficients as brain tissue (Sterenborg et al., 1989). Furthermore, the surface curvature and surrounding tissues and vessels should also be considered. A phantom simulating the complex shape of the brain surface with a tumor should be developed for precise spectral analysis of the fluorescence. Alternatively, an animal in-vivo experiment (i.e., validation study) with pathological analysis of the tumor tissue would overcome the limitations of the experiments using phantoms. The in-vivo testing of spectra measurement and analysis described in the next section showed the actual environment of the in-vivo implementation of the system.

Table 1
Discrimination error at boundary line and accuracy of extraction inside fluorescent region.

Pattern	Discrimination error at boundary lines		Accuracy rate inside fluorescent region (%)
	Average (mm)	Standard deviation	
A	0.02	0.13	99.8
B	−0.01	0.15	98.5
C	0.03	0.10	97.7